Human Molecular Genetics, 2007, Vol. 16, No. 4 ***410–423***
doi:10.1093/hmg/ddl474
Advance Access published on January 8, 2007

Novel pycnodysostosis mouse model uncovers cathepsin K function as a potential regulator of osteoclast apoptosis and senescence

Wei Chen[1,2], Shuying Yang[1,2], Yoke Abe[1], Ming Li[1], Yucheng Wang[1], Jianzhong Shao[1,3], En Li[4] and Yi-Ping Li[1,2,*]

[1]Department of Cytokine Biology, [2]Harvard-Forsyth Department of Oral Biology, The Forsyth Institute & Harvard School of Dental Medicine, 140 The Fenway, Boston, MA 02115, USA, [3]Life Science College, Zhejiang University, Hangzhou, China and [4]Cardiovascular Research Center, Massachusetts General Hospital, Department of Medicine, Harvard Medical School, Charlestown, MA 02129, USA

Received October 18, 2006; Revised and Accepted December 20, 2006

Pycnodysostosis is a genetic bone disease featuring the unique bone homeostasis disorders of osteolysis and osteopetrosis in the same organism. The pathomechanism for pycnodysostosis has been largely unknown due to the unavailability of a pycnodysostosis mouse model with all the traits of the disease. We generated *cathepsin K*$^{-/-}$ mouse strains in the 129/Sv and C57BL/6J backgrounds and found that, only in the 129/Sv background, *cathepsin K*$^{-/-}$ mice exhibit many characteristics of the human pycnodysostosis-like phenotype. Our data indicated that 129/Sv *cathepsin K*$^{-/-}$ osteoclasts (OCs) lacked normal apoptosis and senescence and exhibited over-growth both *in vitro* and *in vivo*. These abnormalities resulted in an unusually high OC number, which is consistent with a recent case study of human pycnodysostosis. Our results show that cathepsin K function has different effects around the skeleton due to site-specific variations in bone homeostasis, such as phenotypes of osteopetrosis in tibiae and osteolysis in calvariae as a result of cathepsin K mutation. Our data demonstrated that the expression levels of *p19*, *p53* and *p21* were significantly reduced in 129/Sv *cathepsin K*$^{-/-}$ OCs and forced expression of *cathepsin K* in pre-OCs induced premature senescence and increased expression of *p19*, *p53* and *p21*. This is the first evidence that cathepsin K plays a key role in OC apoptosis and senescence, revealing the importance of OC senescence in bone homeostasis. The finding of this novel cathepsin K function provides insight into the pathomechanism of pycnodysostosis and may provide new drug targets for diseases involved in OC-related abnormal bone homeostasis.

INTRODUCTION

The cathepsins are a family of cysteine proteases that have been broadly implicated in proteolytic processes during cell growth, cell development and normal adult cellular function. Cathepsins are involved in lysosomal protein degradation, proenzyme activation, antigen processing and hormone maturation. They are secreted by tumor cells, macrophages and osteoclasts (OCs), and they catalyze the remodeling of extracellular matrix proteins. The subclass of cysteine proteases termed lysosomal cathepsins has long been thought to be primarily involved in end-stage protein breakdown within lysosomal compartments. Furthermore, few specific protein substrates for these proteases have been identified. Recently, more cathepsin functions have been discovered. Varela *et al*. (1) reported that cathepsin L marked up-regulation and was associated with the development of senescence phenotypes. Goulet *et al*. (2) showed that cathepsin L functions in the regulation of cell cycle progression.

Cathepsin K was cloned from human osteoclastomas in our laboratory (3) and from rabbit and human OCs in other laboratories (4–7). The important role of *cathepsin K* in OC function was first suggested by the clinical research finding that mutations in this gene caused pycnodysostosis. The human disorder pycnodysostosis is a rare, autosomal, recessive, skeletal disorder caused by mutations in *cathepsin K*

*To whom correspondence should be addressed: Tel: +1 6178928260; Fax: +1 6172624021; Email: ypli@forsyth.org

at 1q21, which codes for cathepsin K, a lysosomal cysteine protease. Mutation in this gene affects the metabolism of the skeletal system, causing defects in bone resorption and bone remodeling (8). In clinical studies, pycnodysostosis is characterized by short stature, osteosclerosis, acroosteolysis, spondylolysis, separated cranial sutures with open fontanelles, bone fragility and loss of mandibular angle (9,10). The *cathepsin K* mutation causes unique pycnodysostosis disorders rather than simple osteopetrosis, as seen in other diseases associated with OC genes such as c-src (11) or Atp6i (12). This feature of the *cathepsin K* mutation suggests that cathepsin K may constitute other functions beyond just matrix protein degradation that could result in the unique phenotypes of pycnodysostosis. Lange and Yutzey (13) reported that endocardial expression of *cathepsin K* in the NFATc1-dependent RANKL signaling pathway is required for heart valve leaflet development and morphogenesis. Godat *et al*. (14) demonstrated that cathepsin K with kinin-degrading properties might act as a kininase, a unique property among mammalian cysteine proteases. Buhling *et al*. (15) showed that early expression of cathepsins B, H and K was found in epithelial cells of the branching presumptive bronchi. The most intense cathepsin K-specific immunoreactivity was found in developing airways with a lumen. Cathepsin K was found only in epithelial cells. In contrast, cathepsins B and H were detected in both epithelial and interstitial cells. These discrete, temporal and spatial variations in *cathepsin* expression during organogenesis of the human lung indicate different physiological roles for the individual enzymes in different cell types and developmental stages.

Four *cathepsin K* knockout mouse strains were generated previously in the outbred 129SVJ-C57BL/6J genetic background (16), the C57BL/6J-BALB/c genetic background (17), the outbred C57BL/6J genetic background (18) and, most recently, another in the C57BL/6J genetic background (19). These *cathepsin K* knockout mice showed mild osteopetrosis, but it was not precisely determined whether they had other pycnodysostosis-like phenotypes, such as acroosteolysis, spondylolysis, separated cranial sutures with open fontanelles and loss of mandibular angle. This suggests that some genetic modifiers of the *cathepsin K* mutation may be present in these strains.

In this study, we generated both a *cathepsin* $K^{-/-}$ 129/Sv inbred strain and a *cathepsin* $K^{-/-}$ C57BL/6J inbred strain. We found that only the 129/Sv inbred strain *cathepsin* $K^{-/-}$ mice mimicked the features of human pycnodysostosis. Recent reports revealing that bone in pycnodysostosis demonstrates increased numbers of OCs, specifically in a young human patient (20,21), prompted us to examine OC number in addition to cathepsin K activity, and to look at the OC phenotype. Our results provide the first evidence that the impairment of normal cathepsin K-mediated OC apoptosis/senescence and matrix protein degradation in *cathepsin* $K^{-/-}$ mice may cause the unique phenotypes of pycnodysostosis. This pycnodysostosis 129/Sv strain mouse model led to the discovery of a novel cathepsin K function as a potential regulator of OC apoptosis and senescence, which may serve as the major feedback mechanism controlling OC numbers in bone homeostasis.

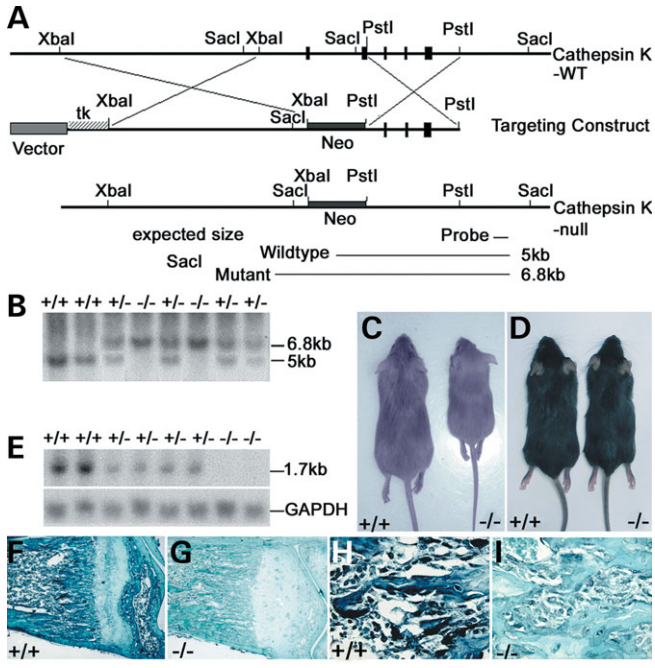

Figure 1. (**A**) Genomic organization of wild-type and targeted alleles after homologous recombination. The targeted allele was produced by replacing the 1.8-kb promoter region, first intron and exons 1 and 2 of the *cathepsin K* gene with a PGK-neo cassette. (**B**) Southern-blot analysis of genomic DNA. Fragments corresponding to wild-type (5 kb) and targeted (6.8 kb) alleles. (C and D) 129/Sv *cathepsin* $K^{-/-}$ mice (**C**, right) were growth retarded when compared with wild-type 129/Sv mice (C, left) and C57BL/J6 mice (**D**). (**E**) Northern blot analysis of *cathepsin K* expression with GAPDH as a control. (F and G) Anti-cathepsin K immunostaining of 129/Sv wild-type and *cathepsin* $K^{-/-}$ tibiae. Expression of *cathepsin K* in wild-type OCs indicated by a black stain (**F**). *Cathepsin* $K^{-/-}$ OCs were not labeled (**G**), confirming the null mutation. (*H,I*) 10× magnifications of (F) and (G), respectively.

RESULTS

Generation of *cathepsin K* null mice in the 129/Sv and C57BL/6J inbred strains

A *cathepsin K* knockout was designed as depicted in Figure 1A. The difference in our design from the four previous reports of knockout mice is that the targeted allele was produced by replacing the 1.8-kb promoter region, first intron and exons 1 and 2 of *cathepsin K* with a PGK-neo cassette to ensure a null mutation.

The widespread occurrence of modifying loci has been documented recently with the generation of novel mutations by gene knockout (22). Because, not all characteristics of the pycnodysostosis phenotype were found in the previous four *cathepsin K* knockout C57BL/6J outbred strains, we made *cathepsin* $K^{-/-}$ 129/Sv and C57BL/6J inbred strains by repeatedly backcrossing for 15 generations with either the 129/Sv or C57BL/6J inbred genetic background to eliminate the interference of modifying loci from different genetic backgrounds and to improve phenotypic consistency.

The *cathepsin K* genotypes of offspring derived from a heterozygote intercross are shown (Fig. 1B). 129/Sv *cathepsin* $K^{-/-}$ mice grew more slowly; their weights were ~30%

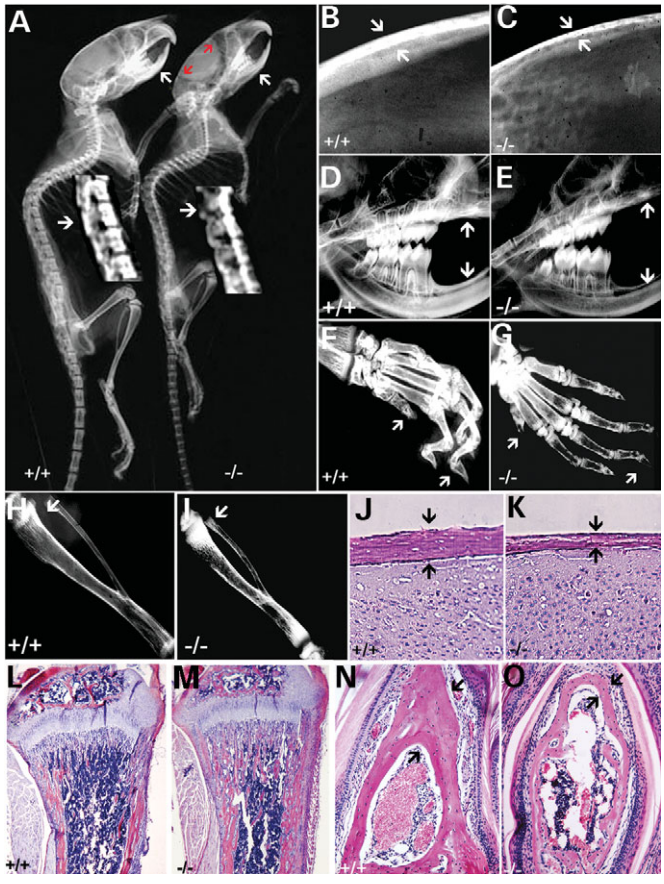

Figure 2. 129/Sv *cathepsin* $K^{-/-}$ mice mimic human pycnodysostosis. (**A**) X-ray analysis of 6-week-old 129/Sv *cathepsin* $K^{+/+}$ and *cathepsin* $K^{-/-}$ mice revealed separated cranial structures (red arrows), loss of mandibular angle (arrows) and spondyolysis of vertebrae (arrows in magnification). (**B** and **C**) The calvariae bone of *cathepsin* $K^{-/-}$ mice (C, arrows) were thin when compared with wild-type mice (B, arrows). (**D** and **E**) *Cathepsin* $K^{-/-}$ mice showed altered bone density and reduced trabeculation of the jawbone, a lack of normal occlusion due to an enhanced open bite (arrows). (**F** and **G**) Acroosteolysis and spondylolysis of the distal phalanges in *cathepsin* $K^{-/-}$ mice when compared with *cathepsin* $K^{+/+}$ mice (arrows). (**H** and **I**) Abnormal marrow cavity in *cathepsin* $K^{-/-}$ mice tibiae (arrow). Increased tibia bone density was also observed. (**J** and **K**) Histological analysis of calvariae from 6-week-old *cathepsin* $K^{+/+}$ and *cathepsin* $K^{-/-}$ mice indicates that the calvariae of *cathepsin* $K^{-/-}$ mice is thinner and the trabecular bone density is reduced (arrows). (**L** and **M**) Histological analyses of tibiae from 6-week-old *cathepsin* $K^{+/+}$ and *cathepsin* $K^{-/-}$ mice illustrate the increased trabeculae present in the bone marrow cavity of the mutant mice (M). (**N** and **O**) Transverse section of the distal phalanges demonstrates acroosteolysis and spondylolysis in *cathepsin* $K^{-/-}$ mice (arrows). $N = 12$.

less than those of their wild-type littermates after 4 weeks (Fig. 1C). However, this difference was not observed in the C57BL/6J genotype (Fig. 1D). A transcript of ~1.7 kb in the *cathepsin* $K^{+/+}$ skeleton total RNA preparation is shown (Fig. 1E). No signal was detected on the RNA preparations of *cathepsin* $K^{-/-}$ skeletons (Fig. 1E), indicating that the *cathepsin K* targeted mutation is a null mutation. Anti-cathepsin K immunostaining of *cathepsin* $K^{+/+}$ and *cathepsin* $K^{-/-}$ mouse tibiae sections using an anti-cathepsin K polyclonal antibody further confirmed the null mutation (Fig. 1F–I).

Table 1. Histomorphometric analysis of the bone from the tibiae (A), calvariae (B), phalanges (C), and vertebrae (D) of 2-week-old control and 129/Sv *cathepsin* $K^{-/-}$ ($Ctsk^{-/-}$) mice ($n = 5$)

	Control	$Ctsk^{-/-}$
(A) Parameter (tibiae)		
Trabecular BV (BV/TV; %)	15.21 ± 5.34	46.15 ± 7.65
OC surface A (Oc.S/TBS; %)	1.32 ± 0.61	16.51 ± 2.78
OC surface B (Oc.S/TAr; %)	0.54 ± 0.26	25.20 ± 6.29
N.Ob/TAr ($/mm^2$)	42.33 ± 8.23	51.23 ± 12.25
(B) Parameter (calvariae)		
Calvariae BV (BV/TV; %)	76.25 ± 4.22	35.65 ± 5.35
OC surface A (Oc.S/TBS; %)	5.54 ± 0.26	30.74 ± 6.29
OC surface B (Oc.S/TAr; %)	3.32 ± 1.54	56.51 ± 5.68
(C) Parameter (phalanges)		
Phalange BV (BV/TV; %)	45.21 ± 4.38	18.18 ± 3.67
OC surface A (Oc.S/TBS; %)	1.22 ± 0.61	12.51 ± 2.63
OC surface B (Oc.S/TAr; %)	0.64 ± 0.36	12.30 ± 6.29
(D) Parameter (vertebrae)		
Vertebrae BV (BV/TV; %)	25.21 ± 5.34	16.15 ± 2.65
OC surface A (Oc.S/TBS; %)	1.32 ± 0.61	16.51 ± 2.78
OC surface B (Oc.S/TAr; %)	0.74 ± 0.38	28.20 ± 7.29

Cathepsin $K^{-/-}$ mice mimic human pycnodysostosis features in the 129/Sv inbred strain and show a lack of bone homeostasis

X-ray analyses of 6-week-old 129/Sv *cathepsin* $K^{-/-}$ mice and C57BL/6J *cathepsin* $K^{-/-}$ mice were performed. Only 129/Sv *cathepsin* $K^{-/-}$ mice exhibited characteristics of pycnodysostosis including short stature, osteopetrosis, acroosteolysis, bone fragility, separated cranial sutures with open fontanelles and loss of mandibular angle (Fig. 2). Of particular interest, we observed spondylolysis, indicated in the *cathepsin* $K^{-/-}$ vertebrae (Fig. 2A). Detailed radiological analyses revealed thin calvariae bones compared with those of wild-type mice (Fig. 2B and C). With respect to tooth development, mutant mice showed altered bone density, reduced jawbone trabeculation, lack of normal occlusion and an enhanced open bite (Fig. 2D and E). There was also a marked deficiency in inter-radicular and alveolar bone heights and a loss of mandibular angle in *cathepsin* $K^{-/-}$ mice when compared with wild-type controls (Fig. 2D and E). Acroosteolysis of the distal phalanges in *cathepsin* $K^{-/-}$ mice in the 129/Sv genotype was consistent with the characteristics of pycnodysostosis (Fig. 2F and G). *Cathepsin* $K^{-/-}$ mice in the C57BL/6J genotype or C57BL/129/Sv hybrid genotype exhibited fewer of these traits associated with pycnodysostosis; they did not show acroosteolysis or spondylolysis of the distal phalanges (data not shown). Radiological analyses also revealed a lack of a normal marrow cavity and increased bone radiodensity in the tibiae of *cathepsin* $K^{-/-}$ mice (Fig. 2H and I). Histological analysis confirmed an increase in the thickness of tibiae bones relative to controls (Fig. 2L and M). In contrast, the histological analysis of 6-week-old *cathepsin* $K^{-/-}$ mice showed thinner calvariae (Fig. 2J and K) and thinner distal phalanges (Fig. 2N and O). The quantitative histomorphometric analysis is shown in Table 1. Thus, the phenotype of *cathepsin* $K^{-/-}$ in the 129/Sv background is noticeably similar to that of a human pycnodysostotic syndrome.

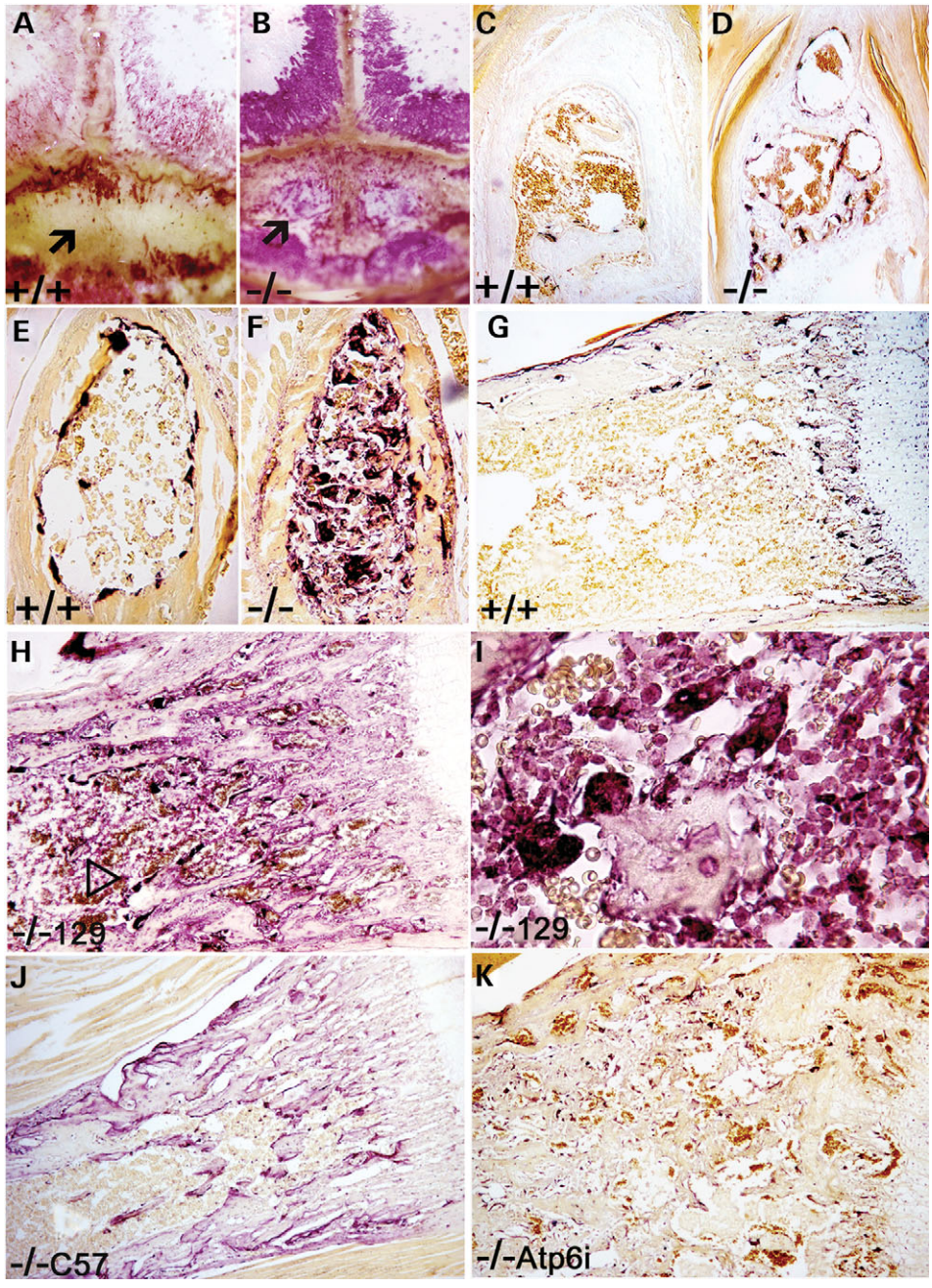

Figure 3. (**A** and **B**) TRAP staining of calvariae in *cathepsin* $K^{+/+}$ and *cathepsin* $K^{-/-}$ mice shows an opening in the calvariae of the *cathepsin* $K^{-/-}$ mice (arrows). (**C** and **D**) TRAP staining in calvariae bone indicates high numbers of OCs in *cathepsin* $K^{-/-}$ mice. The calvariae bones of *cathepsin* $K^{-/-}$ mice were thinner than wild-type mice. (**E** and **F**) TRAP staining in the cross-section of the phalanges shows higher numbers of OCs in *cathepsin* $K^{-/-}$ mice. (**G** and **H**) TRAP staining of wild-type and *cathepsin* $K^{-/-}$ tibiae show high OC numbers in 129/Sv *cathepsin* $K^{-/-}$ tibiae (arrowhead). (**I**) High magnification of 129/Sv *cathepsin* $K^{-/-}$ TRAP-stained tibiae shows mononuclear pre-OCs and multinuclear OCs present within the bone marrow, indicating the loss of normal proliferation controls. (**J**) Slightly increased number of OCs due to slowed apoptosis are visible in the C57BL/6J *cathepsin* $K^{-/-}$ knockout mouse under TRAP staining. (**K**) As a comparison, the *Atp6i*$^{-/-}$ knockout mouse also does not exhibit largely increased numbers of OCs under TRAP staining. $N = 15$.

Extraordinarily high OC numbers in the 129/Sv *cathepsin* $K^{-/-}$ mice, but not in C57BL/6J *cathepsin* $K^{-/-}$ mice or *Atp6i*$^{-/-}$ mice

The availability of a pycnodysostosis mouse model allowed us to study the pathomechanism of pycnodysostosis. First, we examined OC numbers in the mutant mice. All 129/Sv *cathepsin* $K^{-/-}$ mouse bones, including the calvariae (Fig. 3A and B), the distal phalanges (Fig. 3C and D) and the vertebrae (Fig. 3E and F) showed extraordinarily high OC numbers, often more than 15 times higher than that in *cathepsin* $K^{+/+}$ mice, as shown by the quantitative histomorphometric analysis (Table 1B–D). Tartrate-resistant acid phosphatase (TRAP) staining of 129/Sv *cathepsin* $K^{-/-}$

tibiae showed significantly higher OC numbers than wild-type tibiae (Fig. 3G and H). Representative longitudinal sections from the proximal tibiae demonstrated that the number of *cathepsin* $K^{-/-}$ OCs was 15 times higher than the number of wild-type OCs (Fig. 3G and H; Table 1A; Oc.S/TBS). The *cathepsin* $K^{-/-}$ group differs significantly in all three parameters of the quantitative histomorphometric analysis as shown in Table 1. Bone volume/total volume (BV/TV) is about 3-fold higher in trabecular bone and about 2–3-fold lower in other bones. The ratio of OC surface area to bone surface area (Oc.S/TBS) is increased 10–15-fold, and OC surface area as a percentage of the total area (Oc.S/Tar) is increased up to 45-fold compared with littermate controls due to OC growth in bone marrow. No differences were seen in osteoblast number per bone perimeter (N.Ob/B.Pm) or osteoblast surface per measurement field (Ob.S/BS) between *cathepsin* $K^{-/-}$ and control mice (data not shown). Our data in Table 1 demonstrate that bone resorption is down-regulated in the long bones (A) and is up-regulated in calvariae (B), phalanges (C) and vertebrae (D).

The increase in 129/Sv *cathepsin* $K^{-/-}$ OC numbers could be a result of the body compensating for reduced bone-resorbing activity by increasing the number of OCs. To test this possibility, we examined OC numbers in the C57BL/6J *cathepsin* $K^{-/-}$ mice that exhibited mild osteopetrosis and *Atp6i* $^{-/-}$ mice that exhibited severe osteopetrosis. Both C57BL/6J *cathepsin* $K^{-/-}$ mice and *Atp6i* $^{-/-}$ mice only exhibited about a 2-fold increase in OC numbers (Fig. 3J and K). Kiviranta *et al.* (18) reported that the OC surface (Oc.S/BS) was doubled in *cathepsin* $K^{-/-}$ mice in the outbred C57BL/6J genetic background, consistent with our finding in Figure 3J. Our experimental results indicated that any natural capacity that the body has to compensate for low OC activity cannot account for the extreme elevation of OC levels seen in the 129/Sv knockout mice.

Of particular interest is the presence of high numbers of TRAP-positive pre-OCs and OCs within the bone marrow of the 129/Sv *cathepsin* $K^{-/-}$ tibiae (Fig. 3H and I), indicating the over-growth of pre-OCs and OCs that may result from re-entering the cell cycle. To quantify this abundance of pre-OCs and OCs we calculated the ratio of OC surface to total bone area (Table 1, Oc.S/TAr). This observation is the clearest difference between the 129/Sv knockout and both the wild-type control and other strains of knockout mice, C57BL/6J *cathepsin* $K^{-/-}$ mice and *Atp6i* $^{-/-}$ mice, in which mild increases of OCs are only visible along the edges of the trabecular bones (Fig. 3G–K). This is the first observation that TRAP-positive pre-OCs and OCs can grow in the bone marrow mutant mice. The extreme elevation of OC levels seen in the 129/Sv knockout mice indicates that there is another factor affecting the abnormal accumulation of OCs. We hypothesized that this factor could be a novel cathepsin K function in the regulation of OC survival and proliferation that may account for the unique pycnodysostosis features.

Characterization of acidification function and bone resorption activity of *cathepsin* $K^{-/-}$ OCs

To characterize the pathomechanism of pycnodysostosis, we used the pycnodysostosis mouse model to study the nature and function of the *cathepsin* $K^{-/-}$ OCs. We first examined

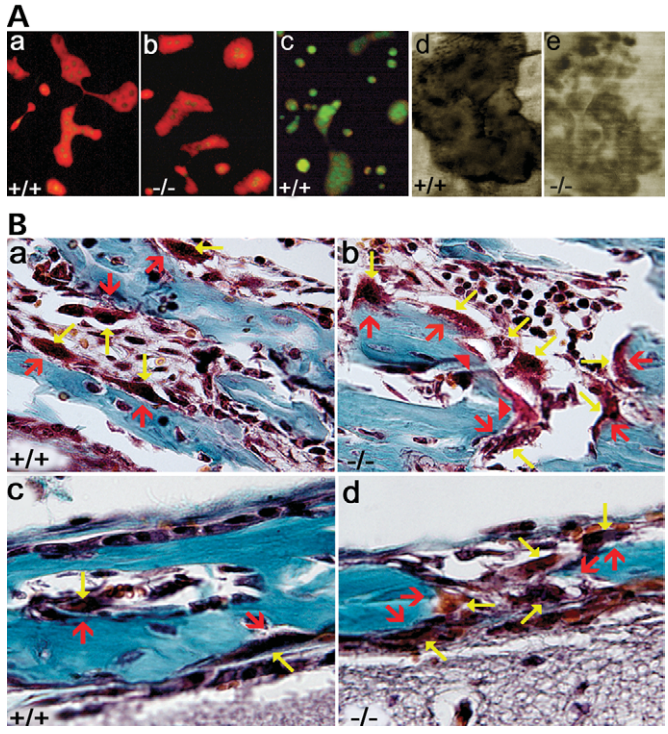

Figure 4. (**A**) Characterization of acidification and bone resorption activity of the OCs deviate between the *cathepsin* $K^{+/+}$ and *cathepsin* $K^{-/-}$ mice. OCL preparations were placed on dentin slices and incubated with acridine orange either without (Aa and b) or with (Ac) NH_4Cl. (Aa and b). Both the cathepsin *cathepsin* $K^{+/+}$ and *cathepsin* $K^{-/-}$ mice showed normal acidification function. (Ac) Orange-positive fluorescence diminished with NH_4Cl, indicating specific staining of acridine orange. (Ad and e) Analysis of OC bone resorption activity in the *cathepsin* $K^{+/+}$ and *cathepsin* $K^{-/-}$ mice. The *cathepsin* $K^{-/-}$ mice (Ae) showed reduced OC resorption activity when compared with the *cathepsin* $K^{+/+}$ mice (Ad), as is evident by the deeper and more sharply defined resorption pit in the *cathepsin* $K^{+/+}$ mice. (**B**) Mutation of *cathepsin K* has varying affects around the skeleton due to site-specific variations in bone homeostasis. High-powered views of bone stained with Goldner's Trichrome, which stains mineralized bone blue-green and osteoids red. Results indicate the variations between wild-type and mutant mouse OCs concerning collagen degradation. OCs are indicated by yellow arrows and their associated lacunas are indicated by red arrows. (Ba and b) The *cathepsin* $K^{+/+}$ tibiae show Howship's lacunae between the OCs and the trabecular bone (Ba), while the *cathepsin* $K^{-/-}$ mice do not have the gap between the OCs and the trabecular bone (Bb), suggesting impaired resorptive capacity. The solid red arrowheads point out areas of collagen that has not been degraded by the OCs even though the OCs have moved further away from the bone (Bb). (Bc and d) Resorption gaps exist between bone and OCs in *cathepsin* $K^{+/+}$ and *cathepsin* $K^{-/-}$ calvariae. However, the *cathepsin* $K^{-/-}$ calvariae have increased levels of OCs (Bd) when compared with *cathepsin* $K^{+/+}$ calvariae (Bc). $N = 8$.

the extracellular acidification function of *cathepsin* $K^{-/-}$ OCs. Both TRAP-positive *cathepsin* $K^{+/+}$ osteoclast-like cells (OCLs) and *cathepsin* $K^{-/-}$ OCLs were obtained. In order to characterize the deficiency in *cathepsin* $K^{-/-}$ OC function, we investigated whether or not extracellular acid compartments were formed in the *cathepsin* $K^{-/-}$ OCLs using the vital stain acridine orange under fluorescence microscopy as described (12,23). Intense orange fluorescence was seen as large, brilliant discs in both *cathepsin* $K^{+/+}$ OCLs (Fig. 4Aa) and *cathepsin* $K^{-/-}$ OCLs (Fig. 4Ab). The orange-positive fluorescence in the (16) OCLs diminished with the

addition of NH_4Cl, indicating specific staining of acridine orange (Fig. 4Ac), as described previously (23). The discs are tentatively attributed to extracellular acidification, implying that *cathepsin K* mutation does not affect the function of OC-mediated extracellular acidification. *Cathepsin* $K^{-/-}$ OCs showed normal acidification functions, suggesting that high numbers of OCs with normal OC-mediated extracellular acidification function may account for the osteolysis at some sites on skeletal bones.

Saftig *et al*. (16) reported that cathepsin K-deficient mice exhibited resorption pits that are shallower and less defined than the controls. To examine bone resorption activity in 129/Sv *cathepsin* $K^{-/-}$ OCs, an *in vitro* OC activity assay was performed. The result showed reduced activity of the OCs in the *cathepsin* $K^{-/-}$ mice (Fig. 4Ae) versus the *cathepsin* $K^{+/+}$ mice (Fig. 4Ad). The difference in shading between the two figures is representative of the difference in the OCs' ability to degrade collagen; the darker shading indicates a deeper, more sharply defined resorption pit (Fig. 4Ad and e). These results indicate that 129/Sv *cathepsin K* mutation did not affect the function of OC-mediated extracellular acidification; however, it did impair the OCs' ability to degrade collagen, as previously reported (16–19).

Mutation of *cathepsin K* has varying effects around the skeleton due to site-specific variations

High numbers of OCs with normal OC-mediated extracellular acidification function may account for the osteolysis, while the impaired ability of OCs to degrade collagen may account for the osteopetrosis. However, we could not explain how osteolysis and osteopetrosis were both occurring in the same organism. We hypothesized that this could be due to differences in various skeletal sites with respect to osteoclastic bone digestion, as reported previously (24). To test this hypothesis, we performed histological analyses of osteoclastic bone digestion from different skeletal sites. *Cathepsin* $K^{+/+}$ tibiae stained with Goldner's Trichrome showed the normal appearance of the OC–bone interface and Howship's lacunae between OCs and trabecular bone (Fig. 4Ba). 129/Sv *cathepsin* $K^{-/-}$ mice did not have Howship's lacunae and exhibited undegraded matrices (Fig. 4Bb), suggesting impaired resorptive capacity. Contrary to what might be expected, the 129/Sv *cathepsin* $K^{-/-}$ knockout did not exhibit the same impairment of bone resorption in the calvariae (Fig. 4Bc and d). The normal lacunae of the OC–bone interface was observed in the 129/Sv *cathepsin* $K^{-/-}$ calvariae, just as it appeared in the 129/Sv *cathepsin* $K^{+/+}$ calvariae (Fig. 4Bc and d). However, as seen in Figure 4Bd, the 129/Sv *cathepsin* $K^{-/-}$ knockout has abnormally high numbers of OCs, which may contribute to the thin calvariae. These observations suggest that while cathepsin K is clearly important to bone resorption in high-turnover long bone, i.e. tibiae (Fig. 2M), cathepsin K is not the critical factor in regulating the bone resorption function of OCs in calvariae. This finding is consistent with a previous report that cathepsin K has little activity in calvarial bone (24).

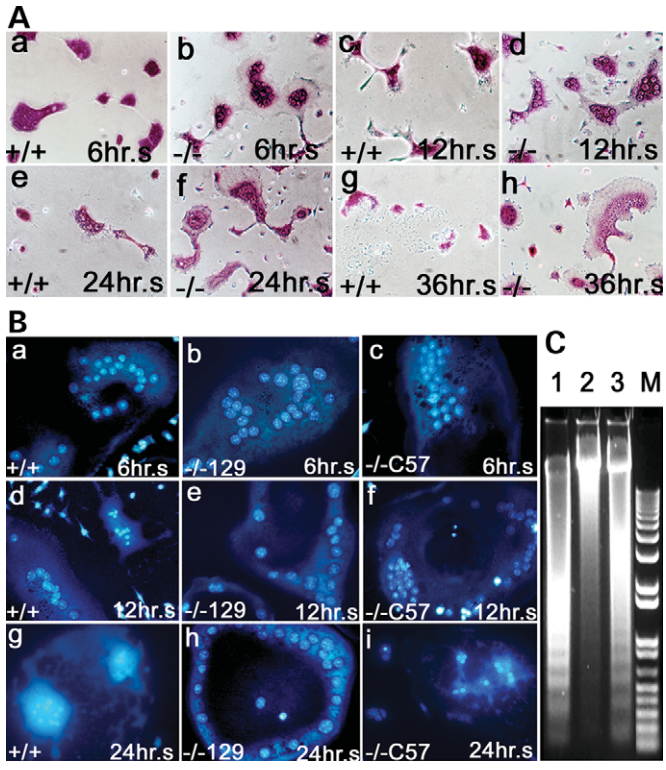

Figure 5. *In vivo* and *in vitro* apoptosis analyses of *cathepsin* $K^{-/-}$ OCs and wild-type OCLs. (**A**) TRAP staining revealed the apoptosis characteristics of *cathepsin* $K^{+/+}$ and *cathepsin* $K^{-/-}$ OCLs cultured for 6 (Aa and b), 12 (Ac and d), 24 (Ae and f) and 36 h (Ag and h). *Cathepsin* $K^{+/+}$ OCLs exhibited apoptosis at 6 h (Aa). *Cathepsin* $K^{-/-}$ OCLs did not exhibit apoptosis until after 36 h (Ah). (**B**) Phase contrast and Hoechst staining images screening for apoptotic morphology and condensed nuclei in OCs from *cathepsin* $K^{+/+}$ (Ba,d and g), 129/Sv *cathepsin* $K^{-/-}$ (Bb,e and h) and C57BL/6J *cathepsin* $K^{-/-}$ (Bc,f and i) mice. Condensed nuclei and apoptosis are evident in the *cathepsin* $K^{+/+}$ cells after 24 h (Bg). The 129/Sv *cathepsin* $K^{-/-}$ cells do not exhibit condensed nuclei or apoptosis (Bh). The C57BL/6J *cathepsin* $K^{-/-}$ cells exhibit condensed nuclei and apoptosis after 24 h (Bi), but apoptosis did not proceed as quickly as in the wild-type (Bg). (**C**) DNA ladder assay for apoptosis. Extensive chromosome degradation is evident in *cathepsin* $K^{+/+}$ cells (lane 1). Chromosome degradation is observed in the C57BL/6J *cathepsin* $K^{-/-}$ cells (lane 3) to a lesser extent than the *cathepsin* $K^{+/+}$ cells. Little or no chromosome degradation is evident in the 129/Sv *cathepsin* $K^{-/-}$ cells (lane 2). $N = 5$.

Impaired apoptosis of *cathepsin* $K^{-/-}$ OCLs

The increased number of OCs in *cathepsin* $K^{-/-}$ mice may result from a defective apoptosis pathway, a high rate of cell proliferation and differentiation, a defective senescence pathway or a combination of all three. To define which mechanism(s) lead to the extraordinarily high number of OCs in *cathepsin* $K^{-/-}$ mice, we first examined apoptosis kinetics in *cathepsin* $K^{-/-}$ OCLs by analyzing the morphological properties of *cathepsin* $K^{+/+}$ and *cathepsin* $K^{-/-}$ OCLs in the 129/Sv mouse strain. We cultured OCs in alpha-modified essential medium containing 10% fetal bovine serum, as described (23), and performed TRAP staining at different times (Fig. 5A). *Cathepsin* $K^{+/+}$ OCLs began to shrink after a 6-h culture, while *cathepsin* $K^{-/-}$ OCLs did not (Fig. 5Aa and b). In addition, the number of apoptosis bodies greatly

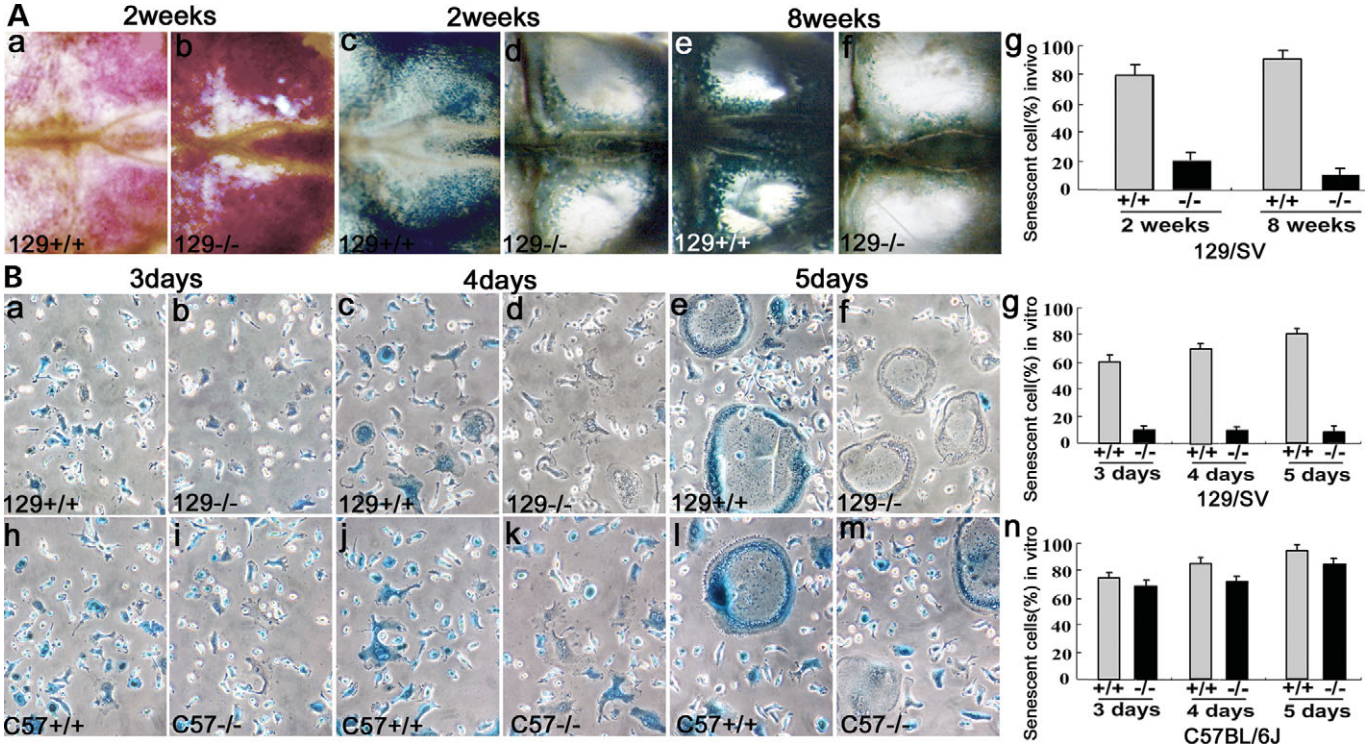

Figure 6. Impaired senescence of *cathepsin* $K^{-/-}$ OCs. (**A**a and b) TRAP staining shows that the number of OCs in *cathepsin* $K^{-/-}$ calvariae is 5.5 times higher than in *cathepsin* $K^{+/+}$ calvariae (Table 1, Oc.S/TBS). (Ac–g) SA-β-gal staining shows extensive blue staining in more than 95% of wild-type OCs by week 8 (Ac,e and g). Blue staining is much less visible in the *cathepsin* $K^{-/-}$ OCs (Ad,f and g). (**B**) *In vitro* culture. (Ba,c,e and g) 60% of *cathepsin* $K^{+/+}$ OCLs were SA-β-gal blue stain positive on day 3, increasing to 85% on day 5. (Bb,d,f and g) 129/Sv *cathepsin* $K^{-/-}$ OCLs were negative for SA-β-gal blue staining on days 3–5. (Bh–n) C57BL/6J *cathepsin* $K^{+/+}$ OCLs and C57BL/6J *cathepsin* $K^{-/-}$ OCLs were SA-β-gal positive on days 3–5. $N = 6$.

increased in *cathepsin* $K^{+/+}$ OCLs in the 12-h culture (Fig. 5Ac and d), in agreement with the previously reported data (25), and no OCs survived through 36 h, whereas many *cathepsin* $K^{-/-}$ OCLs still survived (Fig. 5Ae–h). These observations suggest that *cathepsin* $K^{-/-}$ OCLs have a resistance to apoptosis *in vitro*. Phase contrast and Hoechst staining images were employed using a previously established method (26) to screen for apoptotic morphology and condensed nuclei in OCs from *cathepsin* $K^{+/+}$ (Fig. 5Ba,d and g), 129/Sv *cathepsin* $K^{-/-}$ (Fig. 5Bb,e and h) and C57BL/6J *cathepsin* $K^{-/-}$ mice (Fig. 5Bc,f and i). Condensed nuclei and apoptosis in the *cathepsin* $K^{+/+}$ cells were evident beginning at 6 h and continuing through 24 h (Fig. 5Ba,d and g). The 129/Sv *cathepsin* $K^{-/-}$ cells did not exhibit condensed nuclei or apoptosis even at 24 h (Fig. 5Bb,e and h). The C57BL/6J *cathepsin* $K^{-/-}$ cells exhibited condensed chromosomes and apoptosis similar to *cathepsin* $K^{+/+}$ cells at 6, 12 and 24 h (Fig. 5Bc,f and i). A DNA ladder assay for apoptosis revealed extensive chromosome degradation in *cathepsin* $K^{+/+}$ cells, a finding consistent with the normal apoptosis observed in the *cathepsin* $K^{+/+}$ cells (Fig. 5C, lane 1). Chromosome degradation was observed in the C57BL/6J *cathepsin* $K^{-/-}$ cells to a lesser extent than the *cathepsin* $K^{+/+}$ cells (Fig. 5C, lane 3). The lesser extent of chromosome degradation may explain the mildly increased OC numbers in cathepsin K-deficient mice in the C57BL/6J background established by Kiviranta *et al.* (18). Notably, little or no chromosome degradation was evident in the 129/Sv *cathepsin* $K^{-/-}$ cells (Fig. 5C, lane 2). These results indicated that 129/Sv *cathepsin* $K^{-/-}$ OCs have a resistance to apoptosis *in vitro*.

Impaired senescence of *cathepsin* $K^{-/-}$ OCLs

To address the cause of the extraordinarily high number of OCs, we performed a senescence analysis using SA-β-gal staining, a marker of cell senescence, at pH 6 (27) in the 129/Sv mouse strain. We analyzed OCs in calvariae of 129/Sv mice at 2 and 8 weeks. TRAP staining was performed in order to measure the total number of OCs (Fig. 6Aa and b). Notably, SA-β-gal staining resulted in extensive blue staining in ~90% of wild-type OCs in calvariae by week 8 (Fig. 6Ac,e and g) but staining was much less visible in the OCs of *cathepsin* $K^{-/-}$ calvariae (Fig. 6Ad,f and g). Similarly, in the *in vitro* culture, 85% of 129/Sv *cathepsin* $K^{+/+}$ OCLs were positive for SA-β-gal blue stain by day 5 (Fig. 6Ba,c,e and g), while 129/Sv *cathepsin* $K^{-/-}$ OCLs were negative (Fig. 6Bb,d,f and g). The data demonstrate that *cathepsin K* was associated with senescence in OCs. Interestingly, *cathepsin* $K^{-/-}$ OCLs derived from the C57BL/6J mouse strain were SA-β-gal stain positive on days 3–5 (Fig. 6Bi,k,m and n), similar to C57BL/6J *cathepsin* $K^{+/+}$ OCLs (Fig. 6Bh,j,l and n). This result indicated that impaired senescence in the 129/Sv *cathepsin* $K^{-/-}$ OCLs might be the

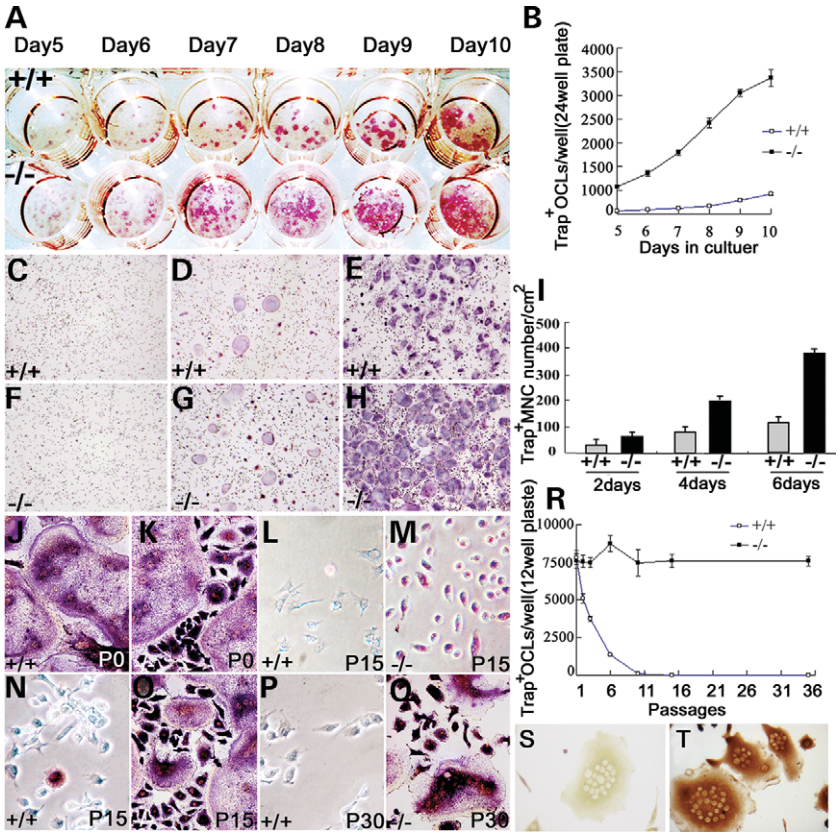

Figure 7. High proliferation rate of *cathepsin* $K^{-/-}$ OCs. (**A**) TRAP staining of *cathepsin* $K^{+/+}$ and *cathepsin* $K^{-/-}$ OCLs cultured in a 24-well plate on different days. (**B**) *Cathepsin* $K^{-/-}$ OCLs grew at more than 10 times the rate of *cathepsin* $K^{+/+}$ OCLs. (**C**–**H**) TRAP staining of multinucleated cell from *cathepsin* $K^{+/+}$ (C–E) and *cathepsin* $K^{-/-}$ (F–H) pre-OCs stimulated by RANKL on days 2 (C and F), 4 (D and G) and 6 (E and H). (**I**) The number of $TRAP^+$ multinucleated cells from *cathepsin* $K^{-/-}$ pre-OCs is double that of *cathepsin* $K^{+/+}$ pre-OCs on all three days. (**J**–**Q**) OCLs induced by pre-OCs in successive passages. (J and K) *Cathepsin* $K^{-/-}$ and *cathepsin* $K^{+/+}$ OCLs from bone marrow showed similar numbers of TRAP-positive cells and morphology. (L and M) TRAP staining of cells from original bone marrow culture passaged 15 times in undifferentiated conditions. *Cathepsin* $K^{-/-}$ cells are still TRAP-positive (M). (O and Q) Upon induced differentiation, *cathepsin* $K^{-/-}$ cells showed TRAP-positive cells and differentiated into OCs. (N and P) OCLs were seldom induced from *cathepsin* $K^{+/+}$ pre-OCs and no TRAP-positive cells were detected. The number of OCs induced from *cathepsin* $K^{+/+}$ pre-OCs decreased 50% after three rounds of passaging, and induced OCs are rarely detected after 10 passages. (**R**) *Cathepsin* $K^{-/-}$ pre-OCs retained the capacity to differentiate through 35 passages. (S and T) OCL controls (**S**) and OCLs immunostained for Atp6i expression with polyclonal antibody serum (**T**) indicate that the passaged cells had retained the capacity to differentiate (12). $N = 7$.

major cause of the extraordinarily high number of OCs in 129/Sv *cathepsin* $K^{-/-}$ mice.

Increased growth of *cathepsin* $K^{-/-}$ OCs

In vivo, high numbers of TRAP-positive pre-OCs and OCs in the bone marrow of the 129/Sv *cathepsin* $K^{-/-}$ tibiae suggested that the pre-OCs and OCs might gain proliferation capacity by re-entering the cell cycle. To test the hypothesis, we performed an *in vitro* OC formation rate assay. *Cathepsin* $K^{+/+}$ and *cathepsin* $K^{-/-}$ OCLs were induced in a bone marrow co-culture system for 10 days as previously described (23). We found that the number of *cathepsin* $K^{-/-}$ OCLs was more than 10 times higher than *cathepsin* $K^{+/+}$ OCLs on a 24-well plate (Fig. 7A and B). This result suggests that *cathepsin* $K^{-/-}$ pre-OCs may have a proliferation potential. As another method of testing for proliferation we stimulated *cathepsin* $K^{+/+}$ and *cathepsin* $K^{-/-}$ pre-OCs with RANKL and performed TRAP staining for multinucleated cells on three different days. The number of $TRAP^+$ multinucleated cells from *cathepsin* $K^{-/-}$ pre-OCs is double that of *cathepsin* $K^{+/+}$ pre-OCs on days 2, 4 and 6 (Fig. 7C–I), indicating significantly accelerated proliferation in *cathepsin* $K^{-/-}$ pre-OCs. To further verify this potential, we subcultured *cathepsin* $K^{+/+}$ and *cathepsin* $K^{-/-}$ pre-OCs and OCs, induced these cells in 10 ng/ml RANKL and 10 ng/ml M-CSF, and performed TRAP staining at different passages. There was no difference in OC numbers from bone marrow primer cultures of wild-type and mutant mice (Fig. 7J and K). Upon induced differentiation with RANKL and M-CSF at passages 15 and 30, differentiated 129/Sv *cathepsin* $K^{-/-}$ pre-OC cells were able to differentiate into OCLs (Fig. 7N–Q), which were characterized by morphological analysis, TRAP staining and Atp6i immunostaining (Fig. 7S and T). Our result showed that *cathepsin* $K^{-/-}$ pre-OCs could be continually passed to 35 passages without losing the pre-OC phenotype and growth capacity (Fig. 7R). In contrast, $<10\%$ of *cathepsin* $K^{+/+}$ pre-OCs were left, compared with *cathepsin* $K^{-/-}$ pre-OCs, at passage 6 (Fig. 7R). *Cathepsin* $K^{+/+}$ pre-OCs almost completely disappeared after passage 10. To test

whether *cathepsin* $K^{-/-}$ pre-OCs can keep their differentiation status, we did TRAP staining for *cathepsin* $K^{-/-}$ pre-OC cells cultured to 15 passages without induction of RANKL. The culture result showed that differentiated 129/Sv *cathepsin* $K^{-/-}$ pre-OC cells can be cultured to 15 passages and still be TRAP positive (Fig. 7L and M). These results suggested that *cathepsin* $K^{+/+}$ pre-OCs could not divide and that *cathepsin* $K^{-/-}$ pre-OCs gained a proliferation capacity and can be continually cultured without loss of pre-OC differentiation status.

Cathepsin K alone is sufficient to initiate senescence in MOCP-5 pre-OC cells

To determine whether *cathepsin K* alone is sufficient to initiate senescence in an immortalized pre-OC cell line, the *cathepsin K* gene was forcefully expressed in MOCP-5 cells (23). We confirmed the forced expression of *cathepsin K* by immunocytochemical staining (Fig. 8Aa and b). Forced expression of *cathepsin K* in MOCP-5 cells resulted in senescence, indicated by positive SA-β-gal staining (Fig. 8Ac–e). Proliferation capacity in MOCP-5 cells with *cathepsin K* over-expression was dramatically decreased (Fig. 8Af). We also investigated whether *cathepsin K* alone is sufficient to initiate senescence in a non-OC cell lineage by over-expressing *cathepsin K* in the rat osteosarcoma cell line, ROS 17/2.8. We confirmed the forced expression of *cathepsin K* in ROS 17/2.8 by immunocytochemical staining (Fig. 8Ag and h). Forced expression of *cathepsin K* in ROS 17/2.8 cells resulted in senescence, shown as positive SA-β-gal staining (Fig. 8Ai–k). Proliferation capacity in ROS 17/2.8 cells with *cathepsin K* over-expression was dramatically decreased (Fig. 8Al). The results were shown as a quantitative comparison of senescence and proliferation capacity of ROS 17/2.8 with and without *cathepsin K* over-expression (Fig. 8Ak and l). The results indicate that *cathepsin K* alone is sufficient to initiate senescence in MOCP-5 pre-OC cells and ROS 17/2.8 cells.

Cathepsin K may regulate OC senescence through the *p19*, *p53* and *p21* senescence pathways

It was reported that apoptosis and senescence may be regulated through the *p19*, *p53* and *p21* pathways in a number of cell types (28,29). To understand the molecular mechanism through which *cathepsin K* regulates OC senescence, we analyzed the expression levels of *p19*, *p53* and *p21* in *cathepsin* $K^{-/-}$ OCLs. As shown in Figure 8B, We found that the expression levels of *p19*, *p53* and *p21* in *cathepsin* $K^{-/-}$ OCLs (lane 2) significantly decreased when compared with those in *cathepsin* $K^{+/+}$ OCLs (lane 1); whereas the expression levels of *p19*, *p53* and *p21* in MOCP-5 cells significantly increased with *cathepsin K* over-expression (lanes 3 and 4). This result indicated that *p19*, *p53* and *p21* are downstream effectors of *cathepsin K* involved in the regulation of OC apoptosis and senescence. Our data suggest that *cathepsin K* mediates OC apoptosis and senescence through the p53-dependent pathway.

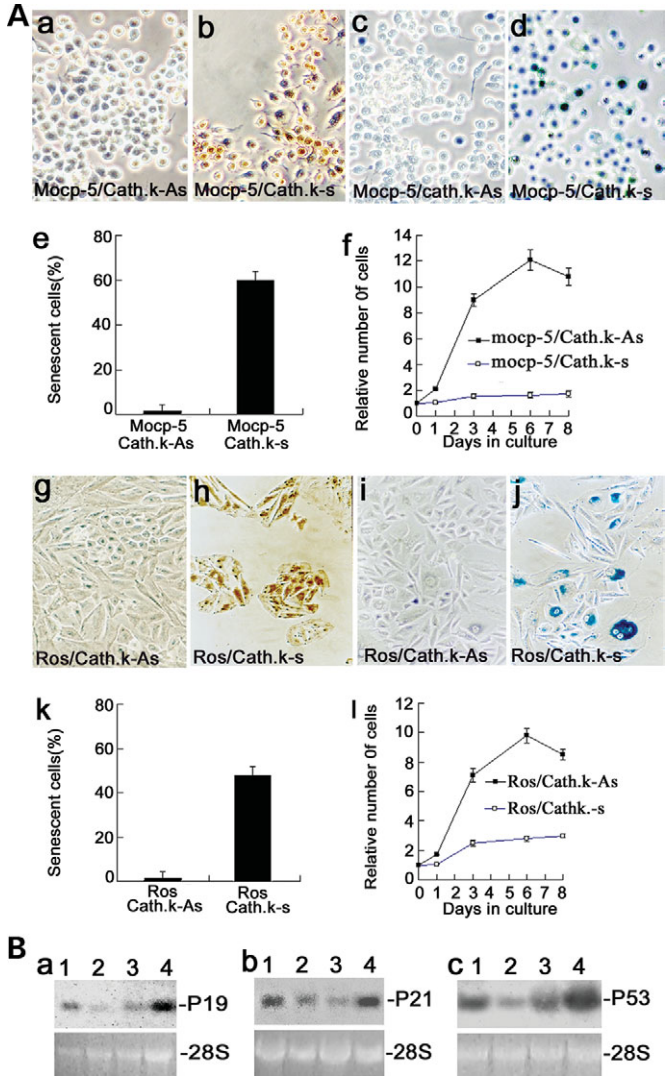

Figure 8. *Cathepsin K*-mediated OC senescence through the *p19*, *p53* and *p21* pathways. (**A**a and b) OCs with forced expression of *cathepsin K*, cathepsin K-sense (Cath. k-s), stained positive by immunocytochemical staining when compared with the control, cathepsin K-anti-sense (Cath. k-As). (Ac and d) *Cathepsin K* forced-expression MOCP-5 cells are *lac*Z stain positive, an indication of senescence (Ad). (Ae and f) Quantitative comparison of senescence in MOCP-5 cells (Ae) indicated that proliferation capacity was lost in MOCP-5/Cath. k-s cells with *cathepsin K* over-expression (Af). (Ag and h) ROS 17/2.8 osteoblast cell negative control (Cath. k-As) shows no staining and the Cath. k-s ROS 17/2.8 osteoblast cells show cathepsin K antibody staining, indicating the presence of cathepsin K expression. (Ai and j) The negative control (Cath. k-As) did not show *lac*Z staining, whereas the Cath. k-s ROS 17/2.8 cells show the blue *lac*Z stain, an indication of senescence. (Ak and l) Quantitative comparison of senescence in ROS 17/2.8 osteoblast cells (Ak) indicated that proliferation capacity was lost in ROS 17/2.8/Cath. k-s cells with *cathepsin K* over-expression (Al). (**B**) Northern blot analysis of *p19* (Ba), *p21* (Bb) and *p53* (Bc) transcripts in *cathepsin* $K^{+/+}$ OCs (lane 1), *cathepsin* $K^{-/-}$ OCs (lane 2), MOCP-5 cells (lane 3) and *cathepsin K* forced-expressed MOCP-5 cells (lane 4). mRNA levels of *p19*, *p21* and *p53* were significantly lower in *cathepsin* $K^{-/-}$ OCs (lane 2) when compared with *cathepsin* $K^{+/+}$ OCs (lane 1). The expression levels of *p19*, *p53* and *p21* were dramatically increased in *cathepsin K*-induced MOCP-5 cells (lane 4) when compared with their control MOCP-5 cells (lane 3). 28s rRNA served as a loading control. Experiments were performed in triplicate ($n = 3$) and three independent experiments yielded similar results ($P < 0.05$).

DISCUSSION

How pycnodysostosis exhibits both osteolysis and osteopetrosis has puzzled bone biologists for many years. We believe that the complicated question has been resolved, for the most part, by this detailed study. In this study we have developed a novel *cathepsin* $K^{-/-}$ mutant mouse strain in the 129/Sv background that resembles human pycnodysostosis. All of our observations of short stature, osteopetrosis, spondylolysis, acroosteolysis, bone fragility, separated cranial sutures with open fontanelles and loss of mandibular angle (Fig. 2) are consistent with the conditions of human pycnodysostosis patients in the report by Edelson *et al*. (30). By comparing the results from the 129/Sv *cathepsin* $K^{-/-}$ mutant mice and from C57BL/6J *cathepsin* $K^{-/-}$ and *Atp6i*$^{-/-}$ mutant mice, we found that the pycnodysostosis phenotype in *cathepsin* $K^{-/-}$ mutant mice is background-dependent. Using this novel pycnodysostosis mouse model, we have deepened our understanding of the pathogenesis of pycnodysostosis and revealed the previously unknown role of cathepsin K as a potential regulator of OC apoptosis and senescence. This unsuspected role of cathepsin K is first evident in the *in vivo* and *in vitro* analyses. The *cathepsin K*-deficient mouse model in the C57BL/6J background, previously established by Kiviranta *et al*. (18), had mildly increased OC numbers compared with the 129/Sv *cathepsin* $K^{-/-}$ knockout mouse model. Using a model similar to theirs in the C57BL/6J background as a control, we found that there is an important difference between previously established mouse models and our 129/Sv *cathepsin* $K^{-/-}$ knockout mouse model, which shows considerably more OCs than both the C57BL/6J *cathepsin* $K^{-/-}$ and *Atp6i*$^{-/-}$ knockouts (Fig. 3). This result demonstrates that the increased OC number in 129/Sv *cathepsin* $K^{-/-}$ mice is not due to simple osteopetrosis, as seen in *Atp6i*$^{-/-}$ mice.

It has been reported that bone in pycnodysostosis demonstrates increased number of OCs (21). Fratzl-Zelman *et al*. (20) analyzed biopsies from a 5-year-old pycnodysostosis patient and found three times as many OCs as in normal biopsies. The 6-week-old mice used in our study are at an equivalent developmental stage to human children, such as this 5-year-old patient. This finding partially supports our assertion that increased OC number in the 129/Sv *cathepsin* $K^{-/-}$ knockout mouse model could be part of the pycnodysostosis phenotype. In our mouse model, we have found that when mice showing the pycnodysostosis phenotype reach 1 year of age, their OC number decreases (data not shown). We speculate that studies of pycnodysostosis using adult patients would also find lower OC numbers and might not link high OC number to the human model of pycnodysostosis.

Mildly increased OC numbers in C57BL/6J *cathepsin* $K^{-/-}$ and *Atp6i*$^{-/-}$ mice (Fig. 3) indicate that the dramatic increase of 129/Sv *cathepsin* $K^{-/-}$ OCs is not due to the body compensating for any decreased efficiency in bone resorption. It seems logical that the body would compensate for reduced bone-resorbing activity by increasing the number of OCs, and this condition is likely to be occurring to a certain extent. However, our experimental results have suggested that the compensatory response of the body cannot account for the extreme elevation of OC levels observed in our knockout mice (Fig. 3, Table 1). Our data indicated that this difference resulted from different OC fates in apoptosis and senescence. Apoptosis and senescence are impaired in the 129/Sv *cathepsin* $K^{-/-}$ knockout OCs (Figs 5 and 6), while apoptosis and senescence function normally in the C57BL/6J *cathepsin* $K^{-/-}$ knockout OCs, indicating the importance of apoptosis and senescence in explaining the difference between the observed OC numbers and underscoring the novelty and significance of our mouse model for understanding the pathogenesis of pycnodysostosis.

Our study demonstrated that cathepsin K has dual functions as a cysteine protease and a regulator of OC survival. The cysteine protease function of cathepsin K in the 129/Sv and C57BL/6J strains is identical. In contrast, the function of cathepsin K as the regulator of OC survival is only essential in the 129/Sv strain. Our results suggest that some genetic modifiers present in the C57BL/6J strain may be able to rescue the pycnodysostotic phenotype that is exhibited in the 129/Sv strain. Similar circumstances involving variation in phenotypes between different mouse strains as a result of genetic variations have been reported in the literature (22,31). Pritchard *et al*. (31) reported the results of a loss-of-function mutation of the X-chromosomal *A-Raf* gene, which caused neurological and intestinal abnormalities and mortality within 21 days postpartum in the C57BL/6J background. However, the mutants in the 129/OLA background did not display intestinal abnormalities, were fertile, survived to adulthood and displayed a subset of the neurological abnormality. Beamer *et al*. (32) also reported a 9% difference in vertebral and 50% difference in femoral adult bone mineral density (BMD) between the C57BL/6J (B6) and C3H/HeJ (C3H) mouse strains. The widespread occurrence of such modifying loci has been emphasized recently with the generation of novel mutations by gene knockout (22,31). Identification of the loci that modify cathepsin K function will require genetic mapping of chromosomal regions that rescue the phenotype defect and may be important for our knowledge of the signal transduction pathways involving OC survival regulation.

Wild-type OCs survived significantly longer in the simulated *in vivo* conditions compared with the *in vitro* conditions (Supplementary Material, Fig. S1). It could be that the 36 h period in which we observed the simulated *in vivo* conditions was not sufficient to disclose a distinction between apoptosis in the wild-type and knockout OCs (Supplementary Material, Fig. S1). Therefore, we should not exclude the possibility of other factors, such as senescence, that might affect OC survival. We found that senescence exists in all wild-type OCs, but is lacking in 129/Sv *cathepsin* $K^{-/-}$ OCs. Because the researchers have focused on the study of apoptosis for OC survival regulation, the importance of senescence in OC survival regulation had not been discovered. The fact that wild-type OCs survived significantly longer in the simulated *in vivo* conditions and that all OCs showed senescence indicate that OC senescence could be the major factor controlling OC numbers in bone homeostasis. Our data demonstrated that the lack of *cathepsin K* causes the 129/Sv *cathepsin* $K^{-/-}$ OCs to re-enter the cell cycle (Fig. 7), whereas forced expression of *cathepsin K* causes premature pre-OC entry into senescence (Fig. 8). These observations provide evidence that *cathepsin K* caused the senescence phenotype observed in wild-type OCs. To our knowledge, our study is the first to report a connection between *cathepsin K* and OC apoptosis and senescence.

We speculate that the observed acroosteolysis, spondylolysis and calvarial thickness may be caused by increased bone resorption due to the presence of large numbers of 129/Sv *cathepsin* $K^{-/-}$ OCs with normal extracelluar acidification function and activity of metalloproteinases. However, this hypothesis cannot explain the osteopetrosis in long bones in pycnodysostosis and the pycnodysostosis-like mouse model. There may be other factors that cause pycnodysostosis-unique osteolysis. Everts *et al*. (24) reported site-specific differences in the skeleton with respect to osteoclastic bone digestion and found that metalloproteinases participate in osteoclastic resorption of calvarial bone but not long bone. We can therefore logically speculate that the extraordinarily high numbers of 129/Sv *cathepsin* $K^{-/-}$ OCs with normal extracellular acidification function and activity of metalloproteinases at the sites where cathepsin K activity is non-essential will result in excessive bone resorption, i.e. osteolysis. The finding by Everts *et al*. that cathepsin K has no activity in the osteoclastic resorption of calvarial bone supports our finding of the similarity in the collagen degradation pattern of *cathepsin* $K^{+/+}$and *cathepsin* $K^{-/-}$ OCs in calvarial bone (Figs 3 and 4). Gowen *et al*. (17) found that C57BL/6J cathepsin K knockouts exhibited osteopetrosis in the long bones, but were relatively unaffected in the calvariae. Gowen *et al*. (17) attributed this difference to the slow bone turnover of calvarial bone compared with long bones, which are high turnover areas that are constantly generating and remodeling bone. Our data indicate that elevated numbers of OCs with no defect in matrix protein degradation in the slow bone turnover sites of 129/Sv cathepsin K knockout mice may cause the observed acroosteolysis, spondylolysis and calvarial thickness. The comparison of 129/Sv and C57BL/6J cathepsin K mutants could elucidate the mechanism underlying osteoclastic bone resorption. While both mutant strains were knockouts of the same gene, each exhibited different phenotypes (Figs 1 and 3). 129/Sv cathepsin K mutant mice exhibited acroosteolysis, spondylolysis and decreased calvarial thickness, while the C57BL/6J did not (data not shown). Thus, we propose that the mechanism underlying acroosteolysis, spondylolysis and calvarial thickness is associated with the relationship between cathepsin K-mediated OC function and number and skeletal site-specific characteristics.

Cathepsin K has been identified as a direct target of the upstream Mitf transcription factor (33). While Mitf is an important regulator of OC gene expression, other transcription factors, such as TFE3, have been identified that can compensate for impaired Mitf function (34,35). Therefore, only Mitf/TFE3 double knockout mice exhibit osteopetrosis. The promoter region of cathepsin K contains three consensus Mitf binding sites, which were deleted in the mutant mouse to prevent a leak of cathepsin K expression. Both microphthalmia (Mitf) and cathepsin (cathepsin K) mutant mice developed osteopetrosis because of the internal relationship among Mitf, cathepsin K and OC function. However, because of their functional differences (Mitf is a transcription factor and cathepsin K is a cysteine protease and OC survival regulator), it is important to note that the double knockout of TFE3 and Mitf is not associated with the features of pycnodysostosis (33–35). As shown in our study, unique pycnodysostosis phenotypes result from a lack of the cathepsin K dual function as a cysteine protease and OC survival regulator.

Previous literature has reported the connection involved in p53-dependent apoptosis and senescence (36). Our data suggest that cathepsin K may mediate OC apoptosis and senescence through the p53-dependent pathway. However, the mechanisms underlying cathepsin K up-regulation of the expression of *p19*, *p53* and *p21* should be explored further. We found that these novel 129/Sv *cathepsin* $K^{-/-}$ mice recapitulated almost all phenotypic alterations observed in pycnodysostotic patients except the double rows of teeth. On the basis of human case reports (30,37–39), we suggest that loss of mandibular angle is a pycnodysostotic phenotype that is common in all affected individuals. The double rows of teeth phenotype has not always been reported and may be less common (37,38). Although the mutant mouse model closely mimics the human genetic condition, it is also possible that the mouse version of the mutation does not exhibit the double rows of teeth phenotype seen in patients due to genetic discrepancies.

In summary, we report the discovery of the novel function of cathepsin K as a potential regulator of apoptosis and senescence. Our data indicated that senescence might be the major pathway controlling *in vivo* OC numbers as a feedback regulator for bone homeostasis. The knockout of cathepsin K exhibits pycnodysostosis due to a combination of the impairment of this novel function as well as the previously established cysteine protease function. The discrepancy between the phenotypes of the 129/Sv and C57BL/6J knockout mice suggests that cathepsin K-mediated apoptosis and senescence is involved in determining the phenotypes of pycnodysostosis. Our results suggest that this novel function of cathepsin K has varying effects around the skeleton due to site-specific variations in bone homeostasis. The combination of the dual functions of cathepsin K in bone homeostasis and site-specific variations in the characteristics of bone can together elucidate the pathogenesis of pycnodysostosis. An improved understanding of the cathepsin K-mediated apoptosis and senescence pathways may provide a new drug target for diseases involved in OC-related abnormal bone homeostasis.

MATERIALS AND METHODS

Cathepsin K gene targeting

The mouse *cathepsin K* genomic DNA was cloned from a 129/Sv genomic library (Stratagene) and the genomic organization determined by Southern blot analysis and DNA sequencing. To generate the *cathepsin K* targeting vector, a 3.8-kb *Xba*I–*Pst*I fragment containing a 1.8-kb promoter region, exons 1 and 2 and intron 1 of the *cathepsin K* gene, was deleted and replaced by a PGK-neo-polyA cassette. The PGK-thymidine kinase gene was inserted into the *Xba*I site. The targeting vector contained 6.0 and 3.0 kb of homologous genomic DNA, respectively, on either side of the neomycin-resistance cassette.

J1 ES cells were transfected with a linearized targeting vector by electroporation and were selected in a medium containing G418 + FIAU, as described previously (40). Two hundred and fifty-four G418/FIAU-resistant ES cell clones

were analyzed by Southern blot hybridization using the genomic fragment next to the *Pst*I fragment as a probe (Fig. 1A), and 22 clones had the targeted allele. Two *cathepsin* $K^{+/-}$ ES clones were injected into C57BL/6J blastocysts to obtain chimeric mice. Germline transmission was achieved by backcrossing with 129Sv and C57BL/6J inbred mice.

Genotype analysis

Genomic DNA was prepared from tails as described (41). For genotype analysis, DNA was digested with *Hin*dIII, blotted and hybridized to genomic probes as indicated in Figure 1A.

mRNA phenotypic assessment

Total RNA was isolated from skeletons of 2-day-old offspring using Chomczynski and Sacchi's method (42). Northern blot analysis of murine *cathepsin K* expression was performed as previously described (23). Briefly, 15 μg of total RNA was fractionated by electrophoresis through 1% agarose/formaldehyde gels followed by northern blot transfer to nitrocellulose membranes pre-soaked in 20× SSC and then covalently bound by baking for 1 h at 80°C, and hybridized with a ^{32}P-labeled fragment of 1.6 kb human *cathepsin K* cDNA as probes (3). After washing, the filters were exposed to X-ray film (Fuji) at −80°C for autoradiography. The same membrane was hybridized with a radioactively labeled GAPDH probe to evaluate the integrity of mRNA and equally loaded in each lane.

Cathepsin K immunostaining

Cathepsin K immunostaining was performed as previously described (23). Briefly, cathepsin K was used to generate an anti-cathepsin K polyclonal antibody in rabbits. The antibody selectively reacts with human and mouse OCs. Mouse tibiae were used for anti-cathepsin K immunostaining. Endogenous peroxidase activity was quenched with 0.3% hydrogen peroxide in methanol for 20 min. Non-specific background staining was blocked by incubating sections in 10% goat serum in PBS for 20 min. Primary antibody (anti-human cathepsin K, 1:100) was applied for 1 h at room temperature. The horseradish peroxidase avidin–biotin complex system (Rabbit Elite ABC Kit, Vector Laboratories) 3,3-diaminobenzidine was used to visualize the bound antibody.

Histological and radiograph procedures

For histological analysis, bones were fixed in 4% paraformaldehyde overnight, and decalcified in 0.5 M EDTA (pH 7.4) for 7–10 days at 4°C, dehydrated in ethanol and embedded in paraffin. Serial sections at 7 μm were stained with hematoxylin/eosin (H/E). For X-ray analysis, we removed the skin of the mice before radiography (high-resolution soft X-ray system). The same radiation energy (30 kV) and exposure times were used for the skeletal elements of both *cathepsin* $K^{+/+}$ and *cathepsin* $K^{-/-}$ mice with high speed holographic film (Kodak).

TRAP staining

Calvariae, vertebrae, tibiae and OCs from *cathepsin* $K^{-/-}$ mice and *cathepsin* $K^{+/+}$ mice and the apoptotic cells were stained with TRAP. TRAP staining was carried out using a commercial kit (Sigma) according to the manufacturer's instructions.

Histomorphometric analysis

Histomorphometric samples were processed as non-decalcified hard-tissue sections as described (18). For quantitative BV histomorphometry, 5 μm sections of 1-week-old mice were stained with Masson–Goldner trichrome (18). For histomorphometric analysis of OC size and number, 10 μm sections of 2-week-old mice were TRAP-stained without counterstaining. Histomorphometric analysis of these sections was performed using the NIH Image J program (43). Three parameters studied in this analysis are presented: the percentage of unresorbed trabecular BV in tibiae relative to the total bone volume (BV/TV), the percentage of OC surface area to total bone surface area of the tibiae, calvariae, phalanges and vertebrae (Oc.S/TBS) and the percentage of OC surface area to the total area of the tibiae, calvariae, phalanges and vertebrae (Oc.S/TAr). Large multinucleated cells with cytoplasmic vesicles and intimate contact to bone were considered as OCs, and cuboidal mononuclear cells in intimate contact with osteoid or bone were identified as osteoblasts.

In vitro osteoclastogenesis

Cathepsin $K^{+/+}$ and *cathepsin* $K^{-/-}$ OCLs were generated as previously described (23). Briefly, *cathepsin* $K^{+/+}$ and *cathepsin* $K^{-/-}$ mice spleen cells were co-cultured with MS12 stromal cells in the presence of 10^{-8} M 1,25$(OH)_2$ vitamin D_3 and 10^{-6} M dexamethasone for 9 days in 24-well plates. $TRAP^+$ OCLs derived from spleen cells were enriched by incubation with 0.2% trypsin for 4 min. After enzyme treatment, more than 95% of the MS12 stromal cells were detached from culture dishes, but all $TRAP^+$ OCLs remained bound. The enriched OCLs were then detached with a plastic scraper after treatment with 0.05% trypsin and 0.02% EDTA for an additional 5 min. *Cathepsin* $K^{+/+}$ and *cathepsin* $K^{-/-}$ OCL preparations were subsequently incubated in α-MEM containing 5 μg/ml of acridine orange (Sigma) for 19 min at 37°C, washed and chased for 10 min in fresh media without acridine orange. Acid production was observed under a fluorescence microscope with a 490 nm excitation filter and a 525 nm arrest filter. For the OCL-conditioned medium culture, supernatant was extracted after 2 days of culture from an MS12 cell co-culture system in the presence of 10^{-8} M 1,25$(OH)_2$ vitamin D_3 and 10^{-6} M dexamethasone without bone marrow cells.

Analysis of pre-OC proliferation

Proliferation of pre-OCs was monitored by OC formation. Mouse BMMs, pre-OCs and OCs were generated as described (44). Isolated BMMs from *cathepsin* $K^{+/+}$ and *cathepsin* $K^{-/-}$ 8-week-old mice were cultured in α-MEM

containing 10% FBS in the presence of 10 ng/ml recombinant M-CSF and 10 ng/ml recombinant RANKL for 48–72 h. BMMs of 5×10^4/well were plated in a 12-well plate. Mature OCs began to form at 96 h of culture. OCs were TRAP-stained at different time points (days 2, 4 and 6) and counted under a microscope.

Bone resorption assay

The bone resorption assay was performed as described (12).

Senescence-associated β-galactosidase (SA-β-gal) staining

SA-β-gal was detected as previously described (27) with slight modifications. Cells were washed once with PBS, fixed for 19 min at 4°C in 2% formaldehyde/0.2% glutaraldehyde, washed four times and incubated with SA-β-gal staining solution [1 mg of 5-bromo-4-chloro-3-indolyl β-D-galactosidase (X-Gal) per milliliter]; 40 mM sodium phosphate, pH 6.0; 5 mM potassium ferrocyanide; 5 mM potassium ferricyanide; 190 mM NaCl; 2 mM $MgCl_2$) overnight at 37°C without CO_2. The quantification of senescent OCLs *in vivo* stained with SA-β-gal was performed using the NIH Image J program (43).

Forced expression of *cathepsin K*

Full-length *cathepsin K* cDNA was subcloned into pCDNA3.1/Zeo for stable transfection in MOCP-5 cells as described (23) or into pCDNA3.1/Neo for stable transfection in ROS 17/2.8 cells as described (45).

Northern blot analysis

Total RNA was extracted using guanidinium thiocyanate, separated on 1.2% agarose, transferred to nitrocellulose and hybridized according to standard procedures with ^{32}P-labeled probes specific for mouse p53, mouse p21 or exon 1b of mouse p19.

Statistical analysis

Statistical significance was evaluated using the Student's *t*-test. The results were considered significant for $P < 0.05$.

SUPPLEMENTARY MATERIAL

Supplementary Material is available at HMG Online.

ACKNOWLEDGEMENTS

We would like to thank Ms Carrie Soltanoff and Mr Lukas Cheney for their assistance with the manuscript. We thank Ms Justine Dobeck for her excellent histological assistance. This work was supported by NIH grant AR-44741 (Y.P.L.), AR-48133–01 (Y.P.L.).

Conflict of Interest statement. None declared.

REFERENCES

1. Varela, I., Cadinanos, J., Pendas, A.M., Gutierrez-Fernandez, A., Folgueras, A.R., Sanchez, L.M., Zhou, Z., Rodriguez, F.J., Stewart, C.L., Vega, J.A. *et al*. (2005) Accelerated ageing in mice deficient in Zmpste24 protease is linked to p53 signalling activation. *Nature*, **437**, 564–568.
2. Goulet, B., Baruch, A., Moon, N.S., Poirier, M., Sansregret, L.L., Erickson, A., Bogyo, M. and Nepveu, A. (2004) A cathepsin L isoform that is devoid of a signal peptide localizes to the nucleus in S phase and processes the CDP/Cux transcription factor. *Mol. Cell*, **14**, 207–219.
3. Li, Y.P., Alexander, M., Wucherpfennig, A.L., Yelick, P., Chen, W. and Stashenko, P. (1995) Cloning and complete coding sequence of a novel human cathepsin expressed in giant cells of osteoclastomas. *J. Bone Miner. Res.*, **10**, 1197–1202.
4. Tezuka, K., Tezuka, Y., Maejima, A., Sato, T., Nemoto, K., Kamioka, H., Hakeda, Y. and Kumegawa, M. (1994) Molecular cloning of a possible cysteine proteinase predominantly expressed in osteoclasts. *J. Biol. Chem.*, **269**, 1106–1109.
5. Bromme, D. and Okamoto, K. (1995) Human cathepsin O2, a novel cysteine protease highly expressed in osteoclastomas and ovary molecular cloning, sequencing and tissue distribution. *Biol. Chem. Hoppe Seyler*, **376**, 379–384.
6. Inaoka, T., Bilbe, G., Ishibashi, O., Tezuka, K., Kumegawa, M. and Kokubo, T. (1995) Molecular cloning of human cDNA for cathepsin K: novel cysteine proteinase predominantly expressed in bone. *Biochem. Biophys. Res. Commun.*, **206**, 89–96.
7. Shi, G.P., Chapman, H.A., Bhairi, S.M., DeLeeuw, C., Reddy, V.Y. and Weiss, S.J. (1995) Molecular cloning of human cathepsin O, a novel endoproteinase and homologue of rabbit OC2. *FEBS Lett.*, **357**, 129–134.
8. Singh, A.R., Kaur, A., Anand, N.K. and Singh, J.R. (2004) Pyknodysostosis: visceral manifestations and simian crease. *Ind. J. Pediatr.*, **71**, 453–455.
9. Johnson, M.R., Polymeropoulos, M.H., Vos, H.L., Ortiz de Luna, R.I. and Francomano, C.A. (1996) A nonsense mutation in the cathepsin K gene observed in a family with pycnodysostosis. *Genome Res.*, **6**, 1050–1055.
10. Gelb, B.D., Shi, G.P., Chapman, H.A. and Desnick, R.J. (1996) Pycnodysostosis, a lysosomal disease caused by cathepsin K deficiency. *Science*, **273**, 1236–1238.
11. Soriano, P., Montgomery, C., Geske, R. and Bradley, A. (1991) Targeted disruption of the c-src proto-oncogene leads to osteopetrosis in mice. *Cell*, **64**, 693–702.
12. Li, Y.P., Chen, W., Liang, Y., Li, E. and Stashenko, P. (1999) Atp6i-deficient mice exhibit severe osteopetrosis due to loss of osteoclast-mediated extracellular acidification. *Nat. Genet.*, **23**, 447–451.
13. Lange, A.W. and Yutzey, K.E. (2006) NFATc1 expression in the developing heart valves is responsive to the RANKL pathway and is required for endocardial expression of cathepsin K. *Dev. Biol.*, **292**, 407–417.
14. Godat, E., Lecaille, F., Desmazes, C., Duchene, S., Weidauer, E., Saftig, P., Bromme, D., Vandier, C. and Lalmanach, G. (2004) Cathepsin K: a cysteine protease with unique kinin-degrading properties. *Biochem. J.*, **383**, 501–506.
15. Buhling, F., Waldburg, N., Kruger, S., Rocken, C., Wiesner, O., Weber, E. and Welte, T. (2002) Expression of cathepsins B, H, K, L, and S during human fetal lung development. *Dev. Dyn.*, **225**, 14–21.
16. Saftig, P., Hunziker, E., Wehmeyer, O., Jones, S., Boyde, A., Rommerskirch, W., Moritz, J.D., Schu, P. and von Figura, K. (1998) Impaired osteoclastic bone resorption leads to osteopetrosis in cathepsin-K-deficient mice. *Proc. Natl Acad. Sci. USA*, **95**, 13453–13458.
17. Gowen, M., Lazner, F., Dodds, R., Kapadia, R., Feild, J., Tavaria, M., Bertoncello, I., Drake, F., Zavarselk, S., Tellis, I. *et al*. (1999) Cathepsin K knockout mice develop osteopetrosis due to a deficit in matrix degradation but not demineralization. *J. Bone Miner. Res.*, **14**, 1654–1663.
18. Kiviranta, R., Morko, J., Alatalo, S.L., NicAmhlaoibh, R., Risteli, J., Laitala-Leinonen, T. and Vuorio, E. (2005) Impaired bone resorption in cathepsin K-deficient mice is partially compensated for by enhanced osteoclastogenesis and increased expression of other proteases via an increased RANKL/OPG ratio. *Bone*, **36**, 159–172.

19. Li, C.Y., Jepsen, K.J., Majeska, R.J., Zhang, J., Ni, R., Gelb, B.D. and Schaffler, M.B. (2006) Mice lacking cathepsin K maintain bone remodeling but develop bone fragility despite high bone mass. *J. Bone Miner. Res.*, **21**, 865–875.
20. Fratzl-Zelman, N., Valenta, A., Roschger, P., Nader, A., Gelb, B.D., Fratzl, P. and Klaushofer, K. (2004) Decreased bone turnover and deterioration of bone structure in two cases of pycnodysostosis. *J. Clin. Endocrinol. Metab.*, **89**, 1538–1547.
21. Helfrich, M.H. (2003) Osteoclast diseases. *Microsc. Res. Technol.*, **61**, 514–532.
22. Smithies, O. (1993) Animal models of human genetic diseases. *Trends Genet.*, **9**, 112–116.
23. Chen, W. and Li, Y.P. (1998) Generation of mouse osteoclastogenic cell lines immortalized with SV40 large T antigen. *J. Bone Miner. Res.*, **13**, 1112–1123.
24. Everts, V., Korper, W., Jansen, D.C., Steinfort, J., Lammerse, I., Heera, S., Docherty, A.J. and Beertsen, W. (1999) Functional heterogeneity of osteoclasts: matrix metalloproteinases participate in osteoclastic resorption of calvarial bone but not in resorption of long bone. *FASEB J.*, **13**, 1219–1230.
25. Kameda, T., Ishikawa, H. and Tsutsui, T. (1995) Detection and characterization of apoptosis in osteoclasts *in vitro*. *Biochem. Biophys. Res. Commun.*, **207**, 753–760.
26. Miyazaki, T., Katagiri, H., Kanegae, Y., Takayanagi, H., Sawada, Y., Yamamoto, A., Pando, M.P., Asano, T., Verma, I.M., Oda, H. *et al*. (2000) Reciprocal role of ERK and NF-kappaB pathways in survival and activation of osteoclasts. *J. Cell Biol.*, **148**, 333–342.
27. Dimri, G.P., Lee, X., Basile, G., Acosta, M., Scott, G., Roskelley, C., Medrano, E.E., Linskens, M., Rubelj, I. and Pereira-Smith, O. (1995) A biomarker that identifies senescent human cells in culture and in aging skin *in vivo*. *Proc. Natl Acad. Sci. USA*, **92**, 9363–9367.
28. Ben-Porath, I. and Weinberg, R.A. (2005) The signals and pathways activating cellular senescence. *Int. J. Biochem. Cell Biol.*, **37**, 961–976.
29. Campisi, J. (2005) Senescent cells, tumor suppression, and organismal aging: good citizens, bad neighbors. *Cell*, **120**, 513–522.
30. Edelson, J.G., Obad, S., Geiger, R., On, A. and Artul, H.J. (1992) Pycnodysostosis. Orthopedic aspects with a description of 14 new cases. *Clin. Orthop. Relat. Res.*, **280**, 263–276.
31. Pritchard, C.A., Bolin, L., Slattery, R., Murray, R. and McMahon, M. (1996) Post-natal lethality and neurological and gastrointestinal defects in mice with targeted disruption of the *A-Raf* protein kinase gene. *Curr. Biol.*, **6**, 614–617.
32. Beamer, W.G., Donahue, L.R. and Rosen, C.J. (2002) Genetics and bone. Using the mouse to understand man. *J. Musculoskelet. Neuronal. Interact.*, **2**, 225–231.
33. Motyckova, G., Weilbaecher, K.N., Horstmann, M., Rieman, D.J., Fisher, D.Z. and Fisher, D.E. (2001) Linking osteopetrosis and pycnodysostosis: regulation of cathepsin K expression by the microphthalmia transcription factor family. *Proc. Natl Acad. Sci. USA*, **98**, 5798–5803.
34. Steingrimsson, E., Tessarollo, L., Pathak, B., Hou, L., Arnheiter, H., Copeland, N.G. and Jenkins, N.A. (2002) Mitf and Tfe3, two members of the Mitf-Tfe family of bHLH-Zip transcription factors, have important but functionally redundant roles in osteoclast development. *Proc. Natl Acad. Sci. USA*, **99**, 4477–4482.
35. Weilbaecher, K.N., Motyckova, G., Huber, W.E., Takemoto, C.M., Hemesath, T.J., Xu, Y., Hershey, C.L., Dowland, N.R., Wells, A.G. and Fisher, D.E. (2001) Linkage of M-CSF signaling to Mitf, TFE3, and the osteoclast defect in Mitf(mi/mi) mice. *Mol. Cell*, **8**, 749–758.
36. Weitzman, J.B., Fiette, L., Matsuo, K. and Yaniv, M. (2000) JunD protects cells from p53-dependent senescence and apoptosis. *Mol. Cell*, **6**, 1109–1119.
37. Everts, V., Aronson, D.C. and Beertsen, W. (1985) Phagocytosis of bone collagen by osteoclasts in two cases of pycnodysostosis. *Calcif. Tissue Int.*, **37**, 25–31.
38. Ho, N., Punturieri, A., Wilkin, D., Szabo, J., Johnson, M., Whaley, J., Davis, J., Clark, A., Weiss, S. and Francomano, C. (1999) Mutations of CTSK result in pycnodysostosis via a reduction in cathepsin K protein. *J. Bone Miner. Res.*, **14**, 1649–1653.
39. Motyckova, G. and Fisher, D.E. (2002) Pycnodysostosis: role and regulation of cathepsin K in osteoclast function and human disease. *Curr. Mol. Med.*, **2**, 407–421.
40. Li, E., Bestor, T.H. and Jaenisch, R. (1992) Targeted mutation of the DNA methyltransferase gene results in embryonic lethality. *Cell*, **69**, 915–926.
41. Laird, P.W., Zijderveld, A., Linders, K., Rudnicki, M.A., Jaenisch, R. and Berns, A. (1991) Simplified mammalian DNA isolation procedure. *Nucleic Acids Res.*, **19**, 4293.
42. Chomczynski, P. and Sacchi, N. (1987) Single-step method of RNA isolation by acid guanidinium thiocyanate–phenol–chloroform extraction. *Anal. Biochem.*, **162**, 156–159.
43. Imbronito, A.V., Todescan, J.H., Carvalho, C.V. and rana-Chavez, V.E. (2002) Healing of alveolar bone in resorbable and non-resorbable membrane-protected defects. A histologic pilot study in dogs. *Biomaterials*, **23**, 4079–4086.
44. Wang, Q., Xie, Y., Du, Q.S., Wu, X.J., Feng, X., Mei, L., McDonald, J.M. and Xiong, W.C. (2003) Regulation of the formation of osteoclastic actin rings by proline-rich tyrosine kinase 2 interacting with gelsolin. *J. Cell Biol.*, **160**, 565–575.
45. Li, Y.P. and Stashenko, P. (1993) Characterization of a tumor necrosis factor-responsive element which down-regulates the human osteocalcin gene. *Mol. Cell. Biol.*, **13**, 3714–3721.